PPAP: Phasing Processing with A Priori

Po-Nan Li
liponan@stanford.edu

Yen-Kai Huang
nykh@stanford.edu

December 10, 2016

1 Introduction

Coherent diffraction imaging (CDI) is a lensless microscopic technique that measures an object's diffraction pattern instead of its direct image [1]. Usually combined with X-ray light source, CDI has been widely used to investigate non-periodic structures of biological cells or nano-particles. While the measured diffraction pattern corresponds to the intensity of Fourier transform (FT) of the original image, the real-space image is only accessible if both its spectral amplitude (square root of the measure intensity) and phase components are available. As a result, a phase retrieval algorithm is required for the image reconstruction.

Several phase retrieval algorithms have been developed for extracting the phase component from oversampled intensity component [3], the most well-known of which is the Hybrid Input-Output (HIO) algorithm [2] (Figure 1(a)). In general HIO was shown to outperform some of the methods that preceded it, such as Error Reduction (ER) , but it usually takes thousands of cycles to converge, and sometimes it stagnates at a suboptimal result. In addition, phasing algorithms like HIO are generally vulnerable to data defects such as quantum noise (for example due to limited photon flux) and missing intensities (for example due to low frequency components being blocked). For the reasons above, performing phase retrieval is generally computationally expensive, because people would run with large iteration numbers to reach optimal reconstruction result.

While a low-resolution image from other microscope sources such as an optical microscope or scanning electron microscope (SEM) is often used to validate reconstruction results, here we propose that we incorporate it, i.e. low-resolution image, into the phase retrieval algorithm as a priori to guide the phasing process. We expect to see the a priori can (i) enhance reconstruction fidelity, (ii) increase convergence rate, and (iii) increase the robustness of phase retrieval against data defects such as quantum noise and missing center.

This project aims to improve upon the HIO algorithm by incorporating a low resolution image as a stronger prior than the finite support constraint used by most algorithms. This should yield a phase retrieval method with a higher reconstruction fidelity and convergence rate, because the LR image contains not only the support boundary but also local intensities information, as well as low-k information in the Fourier domain. Figure 1(b) shows the pipeline we have developed. Given a LR prior of reasonable quality, the modified algorithm in general outperforms the conventional HIO in terms of reconstruction quality and convergence rate. For this project, We researched into different methods for optimizing an image to be closer to the given LR image in a dynamic fashion which can be tuned for convergence, and found indeed the alternating direction methods (ADMs) can be employed to implement phase retrieval algorithms, i.e. HIO [4]. In the following sections, we will briefly review how ADM can be used for phase retrieval, and further develop an ADM approach that employs a LR image to enhance the reconstruction fidelity.

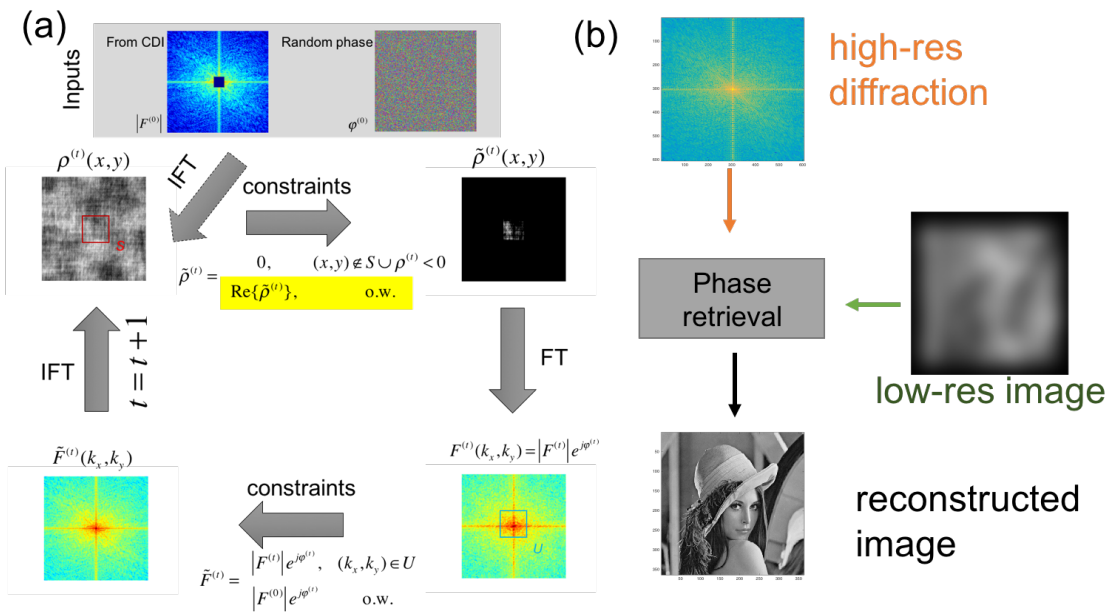

Figure 1: (a) Schematic of the conventional HIO algorithm. The highlighted part indicates the constraint to be studied and improved. (b) Proposed image processing pipeline.

2 Theory background

2.1 HIO

HIO is an iterative method that gradually improves the reconstruction by imposing known properties of the image as constraints. HIO starts with a set of random phases as initial guess, then applies IFT and FT to the image to move it back and forth between real and Fourier spaces. Typically, the constraint for the real space is the fact the image has only a finite support, while the constraint in the Fourier space is that the magnitude of the Fourier image should be close to that measured. Figure 1(a) shows a graph representation of the process.

HIO algorithm was proposed by Fienup [2] to solve a problem of ER algorithm, where ER converge very fast but often converges to suboptimal solutions. HIO algorithm introduces a step length β into the update of the input image $\rho(r)$ based on the desired change in the output image $\rho'(r)$.

$$\rho^{(t+1)}(r) = \begin{cases} \rho'^{(t)}(r) & r \in S \\ \rho^{(t)}(r) - \beta\rho^{(t)}(r) & r \notin S \end{cases} \tag{1}$$

where S denotes the set of points where $\rho(r)$ violates constraints and thus requires a change. This utilizes the special property of the nonlinear system described above that when the input is set to be the current output ($\rho^{(t+1)}(r) = \rho'^{(t)}(r)$) no change will occur in subsequent updates. In the paper, the HIO algorithm was shown to converge much faster than ER algorithm. However, the author agrees there was still some trial and error involved to find the best algorithm for different reconstruction purposes.

A problem with HIO is the fact that one of the two constraint that is associated with the Fourier transform of the optimization variable, in this case the Fourier space constrain, will inevitably be secondary in the process of optimization. The two constraints don't contribute equally to the final result, which can impact the quality of the reconstruction.

2.2 Alternating Direction Methods

Alternating Direction Methods (ADM) is an optimization technique that optimizes a certain variable with many constrains by splitting the variable into multiple copies that each satisfies one constrain, then add constrain that demands the split copies be equal to each other. This seemingly trivial technique is able to balance the contribution of many constraints in the optimization process.

2.2.1 ADM for phase retrieval

Z. Wen *et al.* ([4]) provides an elegant way to formulate the phase retrieval problem in the fashion of optimization. Essentially, the real-space and Fourier-space constraints in the conventional HIO can be formulated as projection operators applied on the split copies of the same image, i.e.

$$\mathcal{P}_s(x) = \begin{cases} x(r) & r \in S \wedge x(r) > 0 \\ 0 & \text{otherwise} \end{cases} \tag{2}$$

where S denotes the bounded support region in the real space, and

$$\mathcal{P}_M(x) = \mathcal{F}^{-1}(\hat{y}),, \text{ where } \hat{y} = \begin{cases} |\hat{x}(r)| \exp j\phi(\hat{x}) & k \in U \\ |b(k)| \exp j\phi(\hat{x}) & \text{otherwise} \end{cases} \tag{3}$$

where $\mathcal{F}$ is the Fourier transform operator and U denotes the missing center in the diffraction plane. We then link the two variable by the constrain that

$$\hat{y} = \mathcal{F}(x) \tag{4}$$

In order to treat the support and the magnitude constraints equally, now we define our problem as follows:

$$\text{find } x \text{ and } y,, \text{ such that } x = y, x \in \mathcal{X} \text{ and } y \in \mathcal{Y}, \tag{5}$$

where $\mathcal{X}$ and $\mathcal{Y}$ are the space of $\mathcal{P}_S$ and $\mathcal{P}_M$, respectively. Now we write down the augmented Lagrangian function for (5)

$$\mathcal{L}(x, y, \lambda) := \lambda^{\mathsf{T}}(x - y) + \frac{1}{2}\|x - y\|^2, \tag{6}$$

where λ is the Lagrangian multiplier. The ADM will now solve the following two subproblems sequentially in each iteration:

$$x^{(t+1)} = \underset{x \in \mathcal{X}}{\operatorname{argmin}} \mathcal{L}(x, y^{(t)}, \lambda^{(t)}) \tag{7}$$

and

$$y^{(t+1)} = \underset{y \in \mathcal{Y}}{\operatorname{argmin}} \mathcal{L}(x^{(t+1)}, y, \lambda^{(t)}), \tag{8}$$

and update the Lagrangian multiplier λ by

$$\lambda^{(t+1)} = \lambda^{(t)} + \beta(x^{(t+1)} - y^{(t+1)}), \tag{9}$$

where the step length β is usually carefully chosen so the iterative algorithm can find the optima while maximizing convergence rate. Since the L-2 norm in (6) is convex and differentiable, it's not difficult to derive the solutions to (7) and (8), which are

$$x^{(t+1)} = \mathcal{P}_{\mathcal{X}}(y^{(t)} - \lambda^{(t)}) \tag{10}$$

and

$$y^{(t+1)} = \mathcal{P}_{\mathcal{Y}}(x^{(t+1)} + \lambda^{(t)}). \tag{11}$$

With (10), (11) and (9), we can implement HIO using the ADM method. The results of this method are presented in Sec. 3.

2.2.2 ADM-HIO with LR prior (PPAP)

In this project we aim to incorporate an LR image into the HIO process. This makes our objective function

$$\mathcal{L}(x, y, \lambda) := \lambda^{\mathsf{T}}(x - y) + \frac{1}{2}\|b - y\|^2, \tag{12}$$

where b represents the LR image. Inspired by the update formula (10), (11) and (9), we propose an alternative update formula by constraining that the real space image x must always be updated to become the LR image

$$\begin{aligned} x^{(t+1)} &= b - \lambda^{(t)} \\ y^{(t+1)} &= \mathcal{P}_{\mathcal{Y}}(x^{(t+1)} + \lambda^{(t)}) \\ \lambda^{(t+1)} &= \lambda^{(t)} + \beta(x^{(t+1)} - y^{(t+1)}). \end{aligned} \tag{13}$$

Here for (13), we replace the $y^{(t)}$ term in the first update equation with the LR image b. Because b is already bounded, we removed the $\mathcal{P}_X$ projection. In principal, we believe this update formulation allowed the LR image to provide a stronger constraint than the binary support mask.

In actual experiments, this update formula yields very interesting results, which are reported in Sec. 3.

2.2.3 TV-regularization

The previous method can sometimes generate a lot of artifacts or false edges when the LR image is of very low quality. The total variation (TV) is a measure of the overall smoothness of an image, defined a

$$V_{\text{aniso}} = \sum_{i,j} |y_{i+1,j} - y_{i,j}| + |y_{i,j+1} - y_{i,j}|$$

Furthermore, we would like to add a TV regularization time in the objective function to ensure reasonable solution. The TV-regularized function might look like

$$\mathcal{L}(x, y, \lambda) := \lambda^{\mathsf{T}}(x - y) + \frac{1}{2}\|b - y\|^2 + \rho\,\Gamma(x), \tag{14}$$

where ρ is a constant deciding the strength of the TV-regularization. So far, it's still unclear to us that whether (12) and (14) make sense. Also, we are now having hard time implementing the TV-regularization term, which is indifferentiable.

3 Results

In this section, we will evaluate the performance of our phase retrieval algorithm, namely PPAP, as well as other three similar algorithms for comparison. We evaluate the output image with the original image ρ_{ideal} that is known by computing the absolute error

$$E_R = \frac{\sum_{(x,y)\in S} |\rho_{\text{out}} - \rho_{idea}|}{\sum_{(x,y)\in S} |\rho_{\text{idea}}|}, \tag{15}$$

where S denotes the sample support, is usually useful for comparing the on-the-fly or final reconstructed image with the model.

Figure 2 shows the E_R evolution of reconstruction by using four different phase retrieval algorithms: conventional HIO by Fienup [2], HIO implemented by ADM [4], image-assisted HIO by one of the authors [5], and the present method, namely PPAP. The first two algorithms only employ the intensity of Fourier transform of the image, shown in Figures 3(a) and 4(a). while the other

two additionally employ a low-resolution version of the target image, shown in Figures 3(b-d) and 4(b-d). Figure 2(a) exhibits that it's unambiguous that our methods outperforms all others, as it quickly converges in first few steps while achieving a super low error if a LR image with $\sigma = 0.01$ is given. If the LR has worse quality, say $\sigma = 0.001$, then PPA stagnates at a mediocre level, while other algorithms that don't use LR can reach low E_R without constraint. We will discuss this limitation in Section sec:discussion. In the following parts we will further assess PPAP with different conditions with multiple parameters.

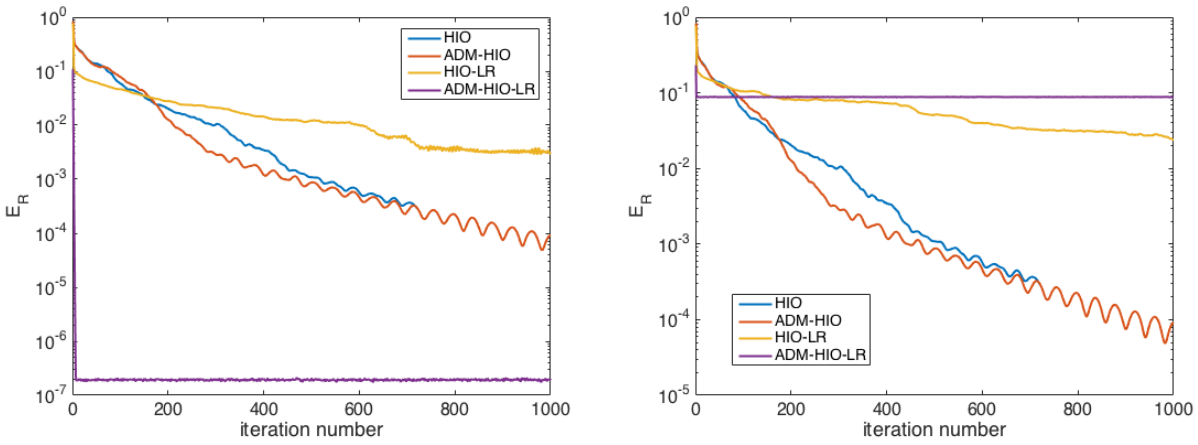

(a) Lena (b) Lena

Figure 2: (a) Lena and (b) mimivirus reconstructed by various phase retrieval algorithms. HIO [2] and ADM-HIO [4] do not use LR, so the results are repeated in every row for comparison. HIO-LR [5] and PPAP were run with LR of different σ: top row $\sigma = 0.01$, middle row $\sigma = 0.001$, bottom row $\sigma = 0.0001$.

3.1 PPAP with different LR qualities

(a) (b) (c) (d)

Figure 3: (a) Simulated diffraction intensity of the Lena photo. (b-d) LR images of $\sigma = 0.01$, $\sigma = 0.001$, and $\sigma = 0.0001$, respectively.

We first evaluated PPAP against LR prior of different qualities. We generated LR images of different qualities by blurring the original image with a Gaussian kernel with a variable bandwidth parameter σ, defined as

$$G = \exp\left(-\frac{k_x^2 + k_y^2}{2\sigma^2}\right) \tag{16}$$

and the LR image is given by

$$\rho_{LR} = \mathcal{F}^{-1}\left[G \cdot \mathcal{F}\rho_{idea}\right], \tag{17}$$

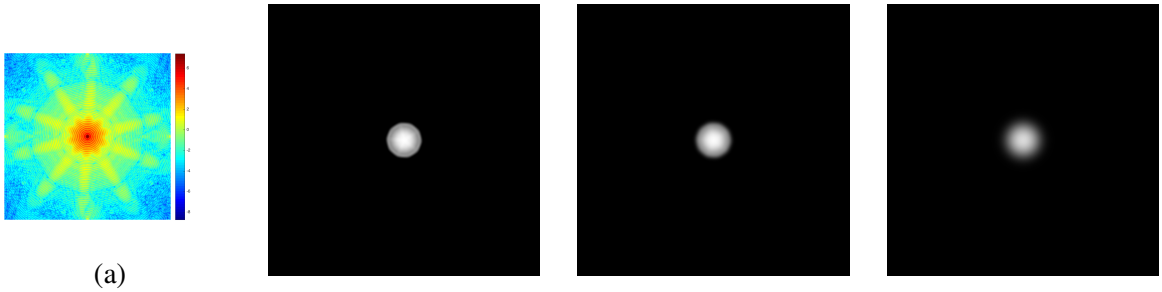

(a) (b) (c) (d)

Figure 4: (a) Simulated diffraction intensity of a mimivirus. (b-d) LR images of $\sigma = 0.01$, $\sigma = 0.001$, and $\sigma = 0.0001$, respectively.

where $\mathcal{F}$ and $\mathcal{F}^{-1}$ denote the Fourier and its inverse transforms respectively. Here we follow the convention that the full-resolution has a resolution up to 0.5 periods, or equivalently bandwidth 1. Hence if we set $\sigma \gg 1$, the filtered image will be almost identical to the original version. Figure 3(b-d) show three LR images with different σ's.

As shown in Figure 5, the HIO-LR and PPAP algorithms are affected by the quality of the LR image. In particular the negative impact on PPAP is very significant, and the reconstructed image comes with many artifacts or false edges in both the Lena and mimivirus images. We propose some possible improvements to solve this problem in Sec. 3.

3.2 Image with quantum noise

We then studied the algorithms' robustness against quantum noise on the diffraction pattern. To simulate the quantum noise, which is the major source of noise in a real CDI image, we rescaled the intensity of the diffraction image to a designed level (in the units of photons per pixel), applied the Poisson distributed noise, then rescaled the diffraction intensity back to the original level to ensure the dynamic range of the image remained in the range of $[0, 1]$. As shown in Figure 6, we see the quantum noise leaves a great impact on the quality of reconstruction result by HIO and ADM-HIO algorithms, while the HIO-LR and PPAP are barely affected. This can be explained because the LR prior that feeds into the reconstruction process was not affected by the same level of quantum noise. Also noteworthy is the fact that the PPAP algorithm and HIO-LR algorithm don't just naively reproduce the LR prior but was able to incorporate information from the noisy diffraction pattern to generate higher resolution.

3.3 Image with missing center

Finally we examined the algorithms' robustness against the missing center scenario. The missing center is a critical limitation for CDI imaging that occurs regardless of the setting of experiment. It occurs because the light source used to cause the diffraction pattern will leave either a projection (with a transparent sample) or a shadow (a opaque sample) in the center of the pattern that blocks the low frequency portion of the diffraction pattern. In the early stage of CDI development, Miao *et al.* have pointed out that the phase retrieval would be impossible if the number of missing components is more than two [3], i.e. two rings in the central part are blocked.

As shown in Figure 7, again the algorithms using an LR prior perform much better in the presence of a simulated missing center. This is more easily explained because the LR prior corresponds to the low frequency component of the original image. The PPAP method shows negligible error in the last row, corresponding to missing center region of 51 pixel in dimension.

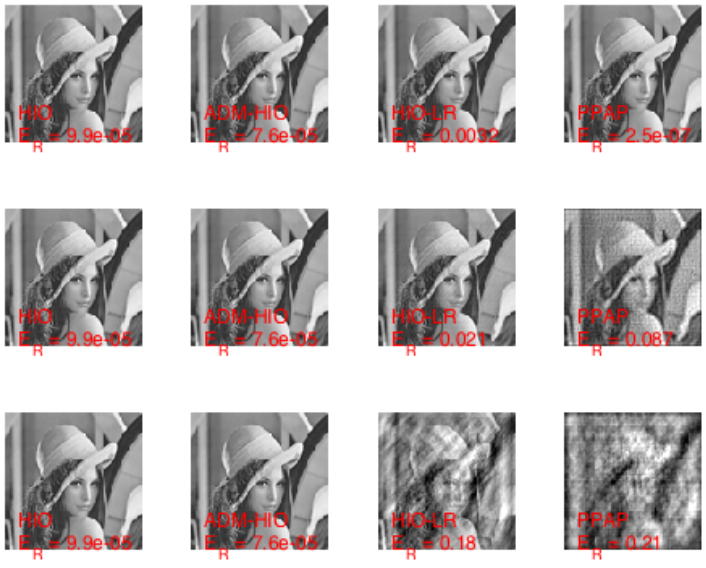

(a) Lena

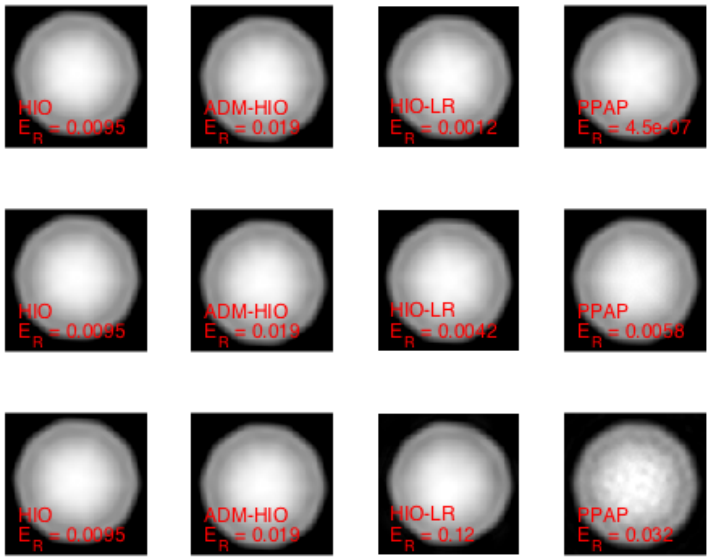

(b) Mimivirus

Figure 5: (a) Lena and (b) mimivirus reconstructed by various phase retrieval algorithms. HIO [2] and ADM-HIO [4] do not use LR, so the results are repeated in every row for comparison. HIO-LR [5] and PPAP were run with LR of different σ: top row $\sigma = 0.01$, middle row $\sigma = 0.001$, bottom row $\sigma = 0.0001$.

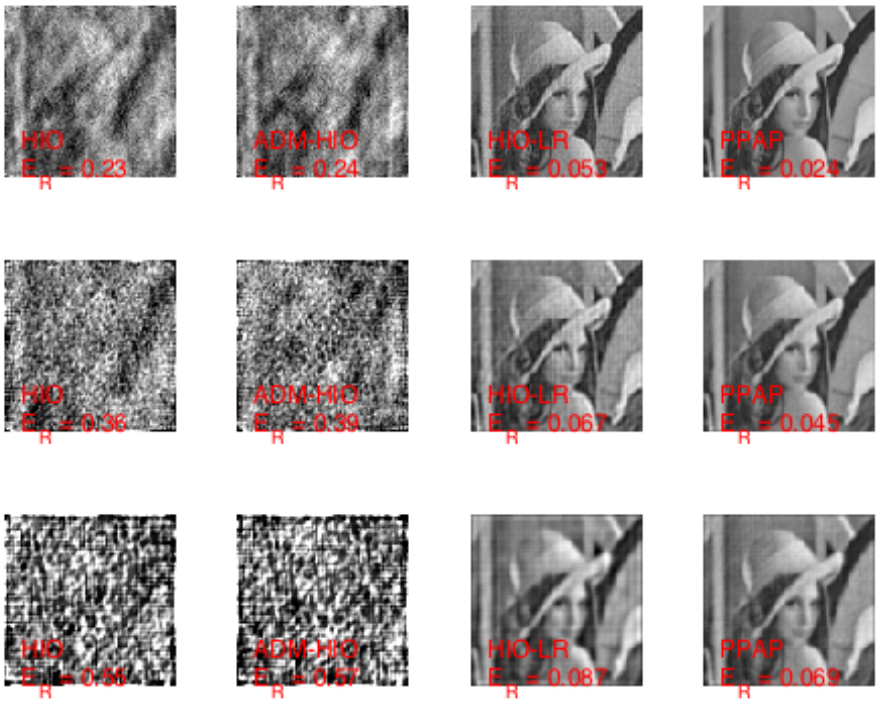

(a) Lena

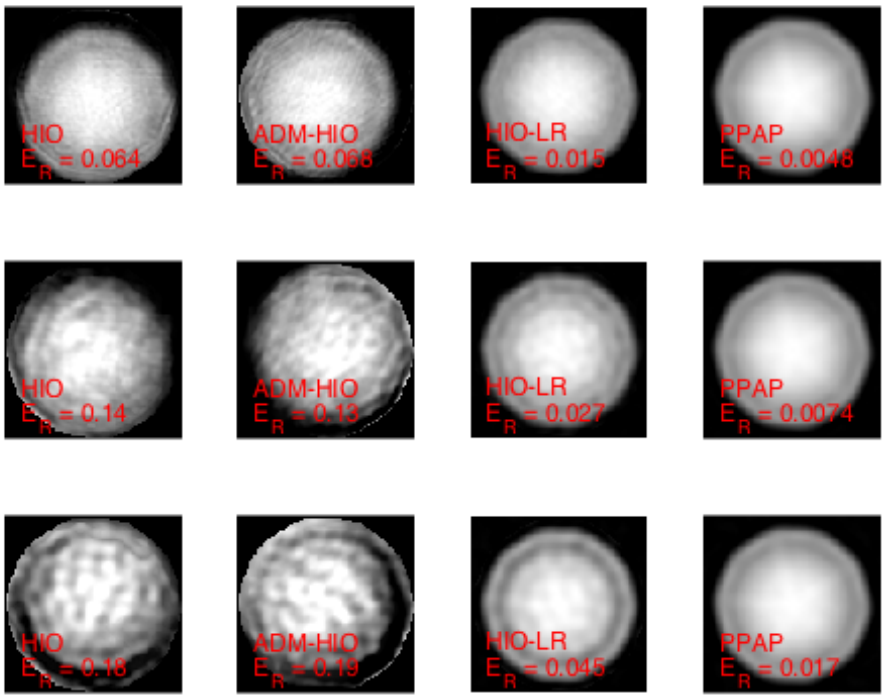

(b) Mimivirus

Figure 6: (a) Lena and (b) mimivirus reconstructed by various phase retrieval algorithms. HIO-LR and PPAP were run with LR of $\sigma = 0.01$. Each row show reconstruction result under different photon flux setting: top row 27.5, middle row 2.75, bottom row 0.275 (photons per second).

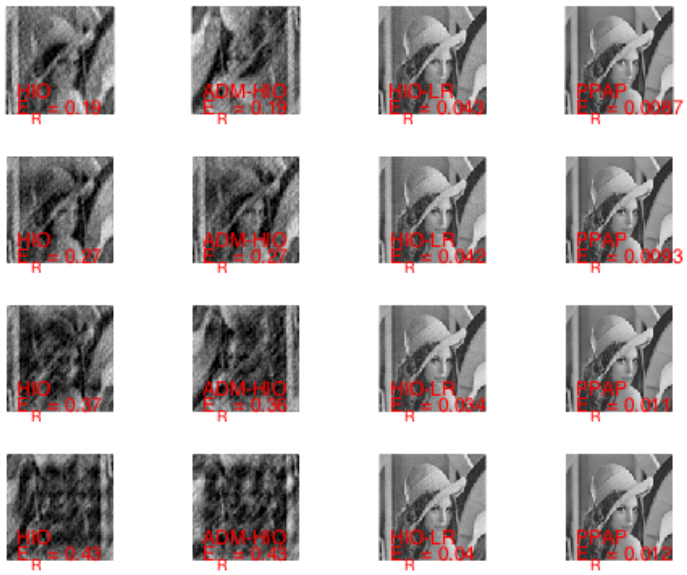

(a) Lena

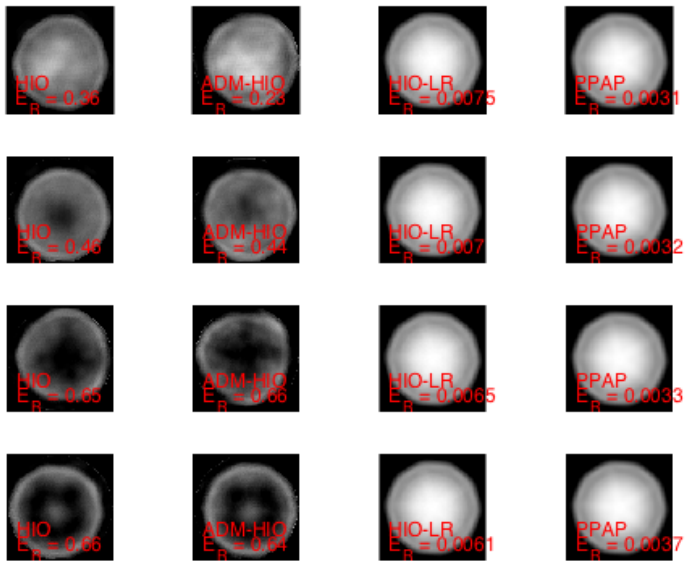

(b) Mimivirus

Figure 7: (a) Lena and (b) mimivirus reconstructed by various phase retrieval algorithms. HIO-LR and PPAP were run with LR of $\sigma = 0.01$. Each row show reconstruction result under different beam stop setting: from top to bottom row correspond to missing 2, 3, 4 and 5 low-k components, respectively. Poisson noise under photon flux 275 photons per pixel was applied to all diffraction patterns.

4 Discussion

In section 3 we admitted that our PPAP method relies on a decent LR image as a priori. For example, we demonstrated that $\sigma = 0.01$, which means the LR only has $1/100$ resolution, would be enough. Certainly in a realistic setting the LR image can be even worse, and as shown in Figure 2(b), PPAP fails in this setting as it is confined by the LR, which is absolutely undesired. To address that, We propose two possible improvements that can potentially enhance the reconstruction result. First, we can add the total variation (TV) of the image as a regularizer to the objective function. As described in Sec. 2.2.3, TV is the sum of variation over the whole image. Intuitively, it measures the "smoothness" of the image. As we have seen previously, the method generates a lot of artifact or false edges when provided with a very low priority prior. If total variation is part of the objective function, we expect the artifacts in the output image to reduce, such that the total variation value in the objective function is small.

The other improvement that might help with the result is to weigh the LR prior in the update formula (13) with a dynamic weight, say γ. That is

$$x^{(t+1)} = \gamma^{(t)} \cdot b - \lambda^{(t)} \tag{18}$$

The weight γ should start out as 1, which makes it identical to (13), but gradually decrease, because as x gradually increase in quality, at some point in the process the LR prior will cease to provide information. Rather the LR prior will start to become the bottleneck to the quality of x. By weighing it with a decreasing dynamic weight $gamma$, we can make the best use of the prior without its negative impact.

Despite the current shortcoming, we believe the current PPAP method can be used to "warm start" other algorithms. We run the PPAP algorithm first and use the result it converges into to initialize some other algorithms. In this way we can save time with phase retrieval algorithms that eventually yield good results but start slowly.

5 Conclusion

In this project we have derived and implemented a new method for phase retrieval that demonstrated very fast convergence given a stronger constraint. This method deserves further study to solidify the mathematical grounding behind the optimization formulation, as well as improvements to stabilize the performance in adverse condition. We think this method has the potential of real application in the field of biological imaging.

Author Contribution

Po-Nan Li conceived this project and implemented the simulation and benchmarking program. Yen-Kai Huang analyzed optimization methods and designed the algorithm. Both authors executed simulations and composed this report.

Matlab code

In addition to the course website of EE368, the code of this project is also publicly available on GitHub [6].

References

[1] J. Miao et al., *Nature* **400**, 342 (1999).

[2] R. Fienup, *Appl. Opt.* **21**, 2758 (1982).

[3] J. Miao et al., *Phys. Rev. Lett.* **95**, 085503 (2005).

[4] Z. Wen, C. Yang, X. Liu, and Stefano Marchesini, *Inverse Prob.* **28**, 115010 (2012).

[5] P.-N. Li et al. (under preparation).

[6] `https://github.com/leeneil/adm`